





Influences of α -clustering configurations on the giant dipole resonance in hot compound systems

S. S. Wang (王闪闪),¹ Y. G. Ma (马余刚) ,^{1,2,*} W. B. He (何万兵) ,^{1,2} D. Q. Fang (方德清) ,^{1,2} and X. G. Cao (曹喜光) ³

¹Key Laboratory of Nuclear Physics and Ion-beam Application (MOE), Institute of Modern Physics, Fudan University, Shanghai 200433, China

²Shanghai Research Center for Theoretical Nuclear Physics, NSFC and Fudan University, Shanghai 200438, China

³Shanghai Advanced Research Institute, Chinese Academy of Sciences, Shanghai 201210, China



(Received 22 January 2023; accepted 29 June 2023; published 19 July 2023)

The influences of α -clustering configurations on the giant dipole resonance (GDR) in hot compound systems are discussed under the framework of an extended quantum molecular dynamics (EQMD) model. The computed GDR spectra in the hot nucleus ^{28}Si are split into two peaks which are very consistent with the experimental measurement and are remarkably sensitive to the configurations of projectile ^{16}O , including the linear chain, kite, square, and tetrahedron configurations. Meanwhile, the sensitivity of the GDR lineshapes to the configurations of ^{16}O gradually increases with angular momentum. However, for the fusion system induced by ^{20}Ne , their GDR lineshapes in ^{47}V and ^{32}S are mostly independent of the α -clustering configurations compared with those in the hot compound systems induced by the projectile ^{16}O , which may be attributed to their much more similar geometric structures between the square pyramid and trigonal bipyramid configurations in ^{20}Ne . Additionally, we find that the GDR lineshapes in hot compound systems are sensitive to the geometric distributions of the projectile in phase space when it is compared to those with Woods-Saxon distribution and polarization in projectiles. These results demonstrate that the GDR can be taken as an experimental observable to extract information about the configurations of reaction systems.

DOI: [10.1103/PhysRevC.108.014609](https://doi.org/10.1103/PhysRevC.108.014609)

I. INTRODUCTION

Clustering structures composed of α clusters, called α -conjugate nuclei, have received widespread attention with the recent rapid development in both theoretical and experimental methods driven by important physics, e.g., exotic structures with α degree of freedom and Bose-Einstein condensation (BEC) in nuclei [1,2]. The larger binding energy per nucleon of an α particle compared to their neighboring light nuclei, along with a strong repulsive α - α interaction due to the Pauli exclusion principle, as well as the symmetry, make the α -clustering states relatively stable in the nuclear environment, which allows for observation of clustering behavior in both excited and ground states [3–5]. As one of the most fundamental physics aspects of light nuclei, α -clustering states play a prominent role in nuclear structure and astrophysics [2,6–20]. Recently, the α -clustering effects were also recognized even in ultrarelativistic heavy ion collisions due to the conversion from initial state coordinate space to final state momentum space [21–26].

Nowadays, several theoretical frameworks have been successfully applied to describe α -clustering configurations in light nuclei and have made some predictions of exotic α -clustering structures. These frameworks include an extended quantum molecular dynamics (EQMD) model [6–8,27–29], covariant density function theory (CDFT) [30,31], time-

dependent Hartree-Fock (TDHF) theory coupled with a density constraint [10,32], fermionic molecular dynamics (FMD) [14], antisymmetrized molecular dynamics (AMD) [15,33,34], and so on. In such α -clustering nuclei, α condensates could be induced as proposed by the THSR (Tohsaki-Horiuchi-Schuck-Röpke) wave function [35], which is analogous to the Bardeen-Cooper-Schrieffer wave function, replacing the Cooper pairs by α particles. Many developments for α -clustering structure have been done within the framework of the THSR wave function [36,37].

The nuclear giant dipole resonance (GDR), as a universal characteristic in the excitation of nuclei throughout the nuclide chart, has been used as an effective probe for gaining key insights into nuclear structure and collective dynamics [38–43]. In heavy deformed nuclei, the GDR spectra are split into two components, providing crucial information about nuclear deformation [43–45]. In the hot compound systems formed by fusion reactions [46,47], the GDR lineshapes at high excitation energies and angular momenta can provide vital information about cluster formation via the study of Jacobi shape transition in rapidly rotating light nuclei, where the shape changes abruptly from noncollective oblate to collective triaxial and/or prolate shape [42,48–50]. In addition, the relationship of the geometrical and dynamical symmetries of α -clustering configurations with the number and centroid energies of peaks in the GDR spectra has been described under the framework of the EQMD model, and it indicates that the GDR can be applied to diagnose different α -clustering configurations in light nuclei [6–8].

*Corresponding author: mayugang@fudan.edu.cn

The aim of this study is to explore the effects of α -clustering configurations on the GDRs in hot compound systems under the framework of the EQMD model. To make comparisons with the experimental measurements, the α -like systems $^{16}\text{O} + ^{12}\text{C}$ and $^{20}\text{Ne} + ^{12}\text{C}$ as well as the non- α -like system $^{20}\text{Ne} + ^{27}\text{Al}$ have been chosen. The paper is organized as follows: In Sec. II, a brief review of the EQMD model and the formula for the GDR are provided. Results and discussion are presented in Sec. III, including the dependence of α -clustering configurations and angular momenta on the GDRs in compound systems induced by α -clustering nuclei, as well as the influences of Woods-Saxon distribution and polarization for projectile at the initial state on the GDRs. Then a summary is given in Sec. IV.

II. MODEL AND FORMALISM

A. Brief review of the EQMD model

The EQMD model, which is developed from the standard quantum molecular dynamics (QMD) [51–54], has some success in investigating giant dipole resonance (GDR) [6–8,43,49,55–57], especially in α -clustering nuclei [6,7,49]. This model improves the description of initial ground states by incorporating the so-called Pauli potential in the effective interaction to approximate the nature of a fermionic many-body system and by treating the width of each nucleon wave packet as an independent dynamical variable [53]. The sufficient stability of the initial ground state obtained within the EQMD model is crucially important to investigate the GDRs in hot compound systems induced by α -clustering nuclei.

In the EQMD model, the total wave function of the system is treated as a direct product of Gaussian wave packets of all nucleons [53],

$$\Psi = \prod_i \varphi(\mathbf{r}_i), \quad (1)$$

$$\varphi(\mathbf{r}_i) = \left(\frac{v_i + v_i^*}{2\pi} \right)^{3/4} \exp \left[-\frac{v_i}{2} (\mathbf{r}_i - \mathbf{R}_i)^2 + \frac{i}{\hbar} \mathbf{P}_i \cdot \mathbf{r}_i \right], \quad (2)$$

where \mathbf{R}_i and \mathbf{P}_i are the centers of position and momentum of the i th wave packet, respectively. The Gaussian width v_i is introduced using a complex as

$$v_i \equiv \frac{1}{\lambda_i} + i\delta_i, \quad (3)$$

where λ_i and δ_i denote the real and the imaginary parts. They are dynamical variables in the process of initialization.

The effective interaction includes Skyrme, Coulomb, and symmetry potentials as well as the Pauli potential. The Pauli potential is written as

$$H_{\text{Pauli}} = \frac{c_p}{2} \sum_i (f_i - f_0)^\mu \theta(f_i - f_0), \quad (4)$$

with $c_p = 15.0$ MeV, $f_0 = 1.0$, and $\mu = 1.3$. The coefficient c_p denotes the strength of the Pauli potential, and θ is the unit step function. f_i is defined as the overlap of the i th nucleon with the other nucleons owning the same spin S and isospin T

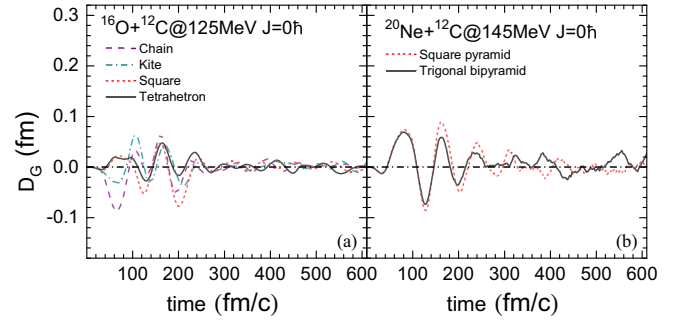


FIG. 1. Time evolution of the dipole moment for ^{28}Si (a) and ^{32}S (b) nuclei, respectively. Different styles of line represent the calculations with different α -clustering configurations of initial projectile nuclei ^{16}O and ^{20}Ne in the present EQMD model.

as follows:

$$f_i \equiv \sum_j \delta(S_i, S_j) \delta(T_i, T_j) |\langle \varphi_i | \varphi_j \rangle|^2. \quad (5)$$

This Pauli potential gives the EQMD model the capability of describing α clustering [6–8,49], which is necessary in our present work.

B. Formula of giant dipole resonance

In 1948, Goldhaber and Teller gave a macroscopic description of giant dipole resonance called the GT mode [58]. They recognized that protons and neutrons behave as two separate rigid but interpenetrating density distributions, and that these two rigid distributions undergo a harmonic displacement with respect to each other at a fixed center of mass [59]. Based on the GT mode, the dipole moment of the system in coordinate space $D_G(t)$ can be represented as [6–8,49,60]

$$D_G(t) = \frac{NZ}{A} [R_Z(t) - R_N(t)], \quad (6)$$

with $R_Z(t)$ [$R_N(t)$] the center of mass for protons (neutrons) in coordinate space. The strength of the giant dipole resonance in the system at excitation energy $E_\gamma = \hbar\omega$ can be determined from the Fourier transformation of the second derivative of $D_G(t)$ with respect to time, i.e.,

$$D''(\omega) = \int_{t_0}^{t_{\text{max}}} D_G''(t) e^{i\omega t} dt, \quad (7)$$

$$\frac{dP}{dE_\gamma} = \frac{2e^2}{3\pi \hbar c^3 E_\gamma} |D''(\omega)|^2, \quad (8)$$

where $\frac{dP}{dE_\gamma}$ is consistent with the γ emission probability.

It is well known that the GDRs critically depend on fusion dynamics (through the timescale for compound nucleus formation) [60]. The initial time t_0 in Eq. (7) corresponds to the moment when the distance between the center of mass of the projectile and target nuclei is approximately the sum of their radii. The final time t_{max} depends on the lifetime of the GDR excitation. For example, Figs. 1(a) and 1(b) show the time evolution of the dipole moment in coordinate space (D_G) for ^{28}Si from the central collision $^{16}\text{O} + ^{12}\text{C}$ at an incident energy 125 MeV and ^{32}S from the central collision $^{20}\text{Ne} + ^{12}\text{C}$ at an

incident energy 145 MeV, respectively. It is seen that they are damped oscillations which can be attributed to both mean-field and two-body collision damping effects. The damped oscillations begin at around 30 fm/c in both of these two collision systems. However, the lifetime of the GDR excitation is apparently different. The former system is exhausted within around 330 fm/c while the lifetime of the latter system is up to 600 fm/c. Therefore, the values of t_0 and t_{\max} in Eq. (7) are variables for different collision systems. It can also be observed that the oscillation frequency associated with the GDR spectrum is sensitive to the α -clustering configurations of the initial projectile nuclei.

III. RESULTS AND DISCUSSION

In the EQMD model, nuclei with $n\alpha$ nucleons at the ground states have α -clustering configurations [6,7], which are sufficiently stable configurations obtained with a cooling procedure coupled with a constraint. ^{16}O , with four α 's, could have four possible structures, including linear chain, kite, square, and tetrahedron configurations. ^{20}Ne with five α 's can have square pyramid and trigonal bipyramid configurations, and shows possible evidence of the existence of the 5α condensate state above the 5α threshold [61]. For ^{12}C , there are linear chain and regular triangle configurations. Since the three- α regular triangle configuration of ^{12}C at the ground state has been predicted by antisymmetrized molecular dynamics (AMD) [15], fermionic molecular dynamics (FMD) [14], and covariant density functional theory [9], as well as a recent experimental measurement which presents evidence for triangular D_{3h} symmetry in the ground state of ^{12}C [13], we only select ^{12}C with regular triangle configuration as the target nucleus in the collisions of $^{16}\text{O} + ^{12}\text{C}$ and $^{20}\text{Ne} + ^{12}\text{C}$ in our present work. It should be noted that the orientations of projectile and target nuclei in phase space are random at initial states in our calculations.

A. α -clustering configuration dependence

It is well known that the initial projectile and target structures play an important role in forming compound nuclei, especially those with exotic geometric structure. Recent experiments and theoretical calculations indicate that α clustering has an effect on the GDRs in hot compound systems induced by α -conjugate nuclei [42,48,49]. In this section, we focus on the α -clustering configuration dependence of GDRs in hot compound systems.

Figure 2 shows the GDR spectra computed within the EQMD model for both the hot rotating nuclei ^{28}Si and ^{47}V with a high angular momentum. Here the angular momentum J is closely related to the impact parameter b , i.e.,

$$b = \frac{J}{\frac{A_r A_p}{A_r + A_p} \sqrt{2m_0 E_{\text{int}}}}, \quad (9)$$

where $m_0 = 938.3 \text{ MeV } c^{-2}$, A_p (A_t) is the mass number of projectile (target) nucleus, respectively, and E_{int} denotes the incident energy per nucleon. Different style curves correspond to the GDR spectra of hot rotating nuclei from fusion reactions induced by α -conjugate projectiles with different

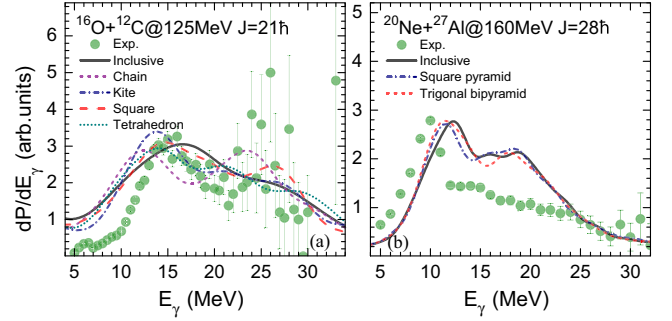


FIG. 2. The GDR spectra computed within the EQMD model for ^{28}Si (a) and ^{47}V (b) nuclei along with the experimental data (solid symbols).

α -clustering configurations. Black solid lines refer to the GDR spectra computed within the EQMD model based on the inclusive collision events where projectile nuclei own all different configurations initialized by the EQMD model. Solid symbols denote experimentally measured GDR spectra performed at the Variable Energy Cyclotron Centre (VECC), Kolkata [48,62], and show that a two-component GDR spectrum for ^{28}Si confirms its highly extended prolate shape, and the spectrum with a narrow peak around 10 MeV for ^{47}V is a signature of the Jacobi shape transition.

In Fig. 2(a), the hot rotating nucleus ^{28}Si originates from the fusion reaction $^{16}\text{O} + ^{12}\text{C}$ with angular momentum $J = 21\hbar$ at incident energy 125 MeV. For projectile ^{16}O , we take into account the linear chain, kite, square, and tetrahedron configurations as well as inclusive configurations. It can be seen that the computed GDRs' spectra in the hot rotating nucleus ^{28}Si are similar to the experimental data, which have two peak components located at about $E_\gamma = 15$ and 25 MeV. The cluster components in the initialized projectile and target can be amplified in the fusion process, where the cluster degree of freedom is well developed, though the clusters overlaps with each other in initialization. However, the GDR lineshapes from several systems are different and are sensitive to the α -clustering configurations of the projectile ^{16}O . This indicates that the experimental data may have been extracted from a reaction system induced by mixed α -clustering configurations of the projectile.

In Fig. 2(b), the hot rotating nucleus ^{47}V comes from the $^{20}\text{Ne} + ^{27}\text{Al}$ systems with angular momenta $J = 28\hbar$ at incident energy 160 MeV. All of the GDR calculations, including those of the inclusive, square pyramid, and trigonal bipyramid configurations in projectile ^{20}Ne , display a narrow peak at lower energy similarly to the experimentally extracted spectrum. However, when compared with the experimental data, these narrow peak positions in our calculations are located at a higher energy, 11.5 MeV, and there is apparently another peak at $E_\gamma = 19.0$ MeV. It may be due to the quantum fluctuation that is not large enough in the EQMD model compared with the realistic case. The phase space shape will be more diverse if the fluctuation can be enhanced, which perhaps will improve the GDR computed result. Additionally, one can observe that the GDR spectrum in ^{47}V is hardly sensitive to the

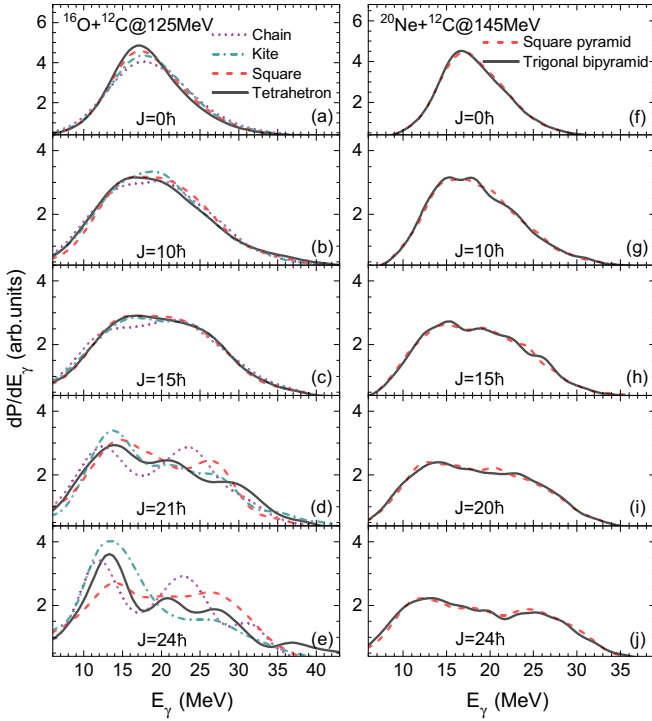


FIG. 3. The GDR spectra computed within the EQMD model for ^{28}Si (a)–(e) and ^{32}S (f)–(j) nuclei with angular momentum J from $0\hbar$ to $24\hbar$.

α -clustering configurations of the projectile ^{20}Ne , probably due to their similar geometric configurations.

B. Angular momentum dependence

A rapidly rotating light nucleus in general is oblate at low angular momentum J , and its deformation increases with J . Above a certain critical J_c near the fission limit, the shape changes abruptly from noncollective oblate to collective triaxial and/or prolate shape characterized by larger deformations. This phase transition is similar to the one that occurs in gravitating rotating stars where the Jacobi transitions are predicted to occur beyond a certain critical angular momentum J_c . In this section, we will discuss the angular momentum dependence of the GDRs in hot rotating nuclei from the fusion reactions between two α -conjugate nuclei.

Under the framework of the EQMD model, we calculate the GDR spectra in the hot compound nuclei ^{28}Si and ^{32}S with angular momenta J from $0\hbar$ to $24\hbar$, which are plotted in Fig. 3. For the $^{16}\text{O} + ^{12}\text{C}$ reaction at incident energy 125 MeV in Figs. 3(a)–3(e), we consider four α -clustering configurations for the α -conjugate projectile ^{16}O labeled by different style lines, including the linear chain, kite, square, and tetrahedron configurations, and a regular triangle configuration for the target ^{12}C . It is noteworthy that all of the GDR spectra shapes for the different α -clustering configurations in ^{16}O are mostly similar at $J < 15\hbar$, whereas with increasing J the GDR spectra in the hot rotating nucleus ^{28}Si become more sensitive to the α -clustering configurations in the projectile ^{16}O . Interestingly, as seen from Figs. 3(f)–3(j),

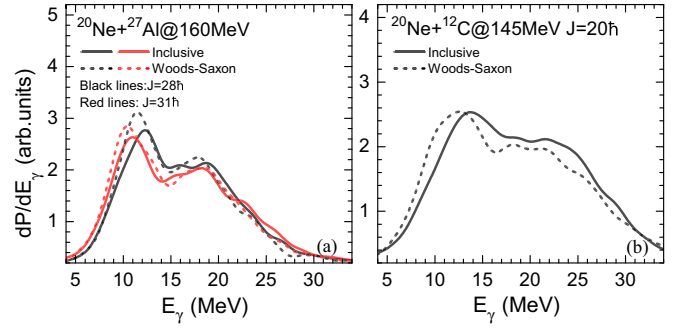


FIG. 4. The GDR spectra obtained within the EQMD model for ^{47}V (a) and ^{32}S (b) nuclei. The calculations with inclusive projectile nuclei are shown as solid lines, and dotted lines correspond to those of projectile nuclei with the Woods-Saxon configuration.

the GDRs in the hot compound nucleus ^{32}S from the fusion reaction $^{20}\text{Ne} + ^{12}\text{C}$ at incident energy 145 MeV are mostly independent of the α -clustering configurations in the projectile ^{20}Ne . This is because the two geometric structures for the α -conjugate projectile ^{20}Ne , i.e., square pyramid and trigonal bipyramid configurations, are much more similar than those among the four different configurations in the projectile ^{16}O at a given J . Furthermore, the GDR spectrum widths in the hot compound nuclei ^{28}Si and ^{32}S show a gradually increasing trend with increasing angular momentum J , which is consistent with the experiments. It is found experimentally that GDR width keeps almost constant for low spin values while the width increases obviously in the high angular momentum region [63,64]. Additionally, one can observe that the GDR spectra in the hot rotating nucleus ^{28}Si with $J = 24\hbar$ display a narrow peak at around $E_\gamma = 13.5\text{MeV}$ for the kite and tetrahedron structures in the projectile ^{16}O in Fig. 3(e), which hints that they may undergo the Jacobi shape transition.

C. Woods-Saxon effects

The GDR spectrum shapes can reflect the initial geometric configurations of the projectile. In this section, we focus on studying the effects of the Woods-Saxon distribution on the GDR spectra in hot rotating nuclei from fusion reactions.

Figure 4 shows the GDR spectra in hot rotating nuclei ^{47}V and ^{32}S computed within the EQMD model. Solid lines represent the results from the fusion reactions induced by the projectile with the inclusive configurations, and dotted lines correspond to those from the reactions induced by the projectile with the Woods-Saxon configuration. For the ^{47}V from the system $^{20}\text{Ne} + ^{27}\text{Al}$ at 160 MeV, these GDR spectra have a sharp peak component at a lower E_γ [see Fig. 4(a)], which is in conformity with the experimental measurement [48], indicating that the compound nucleus ^{47}V undergoes a Jacobi phase transition. Meanwhile, it is found that the narrow peak position at $J = 31\hbar$ appears at a lower E_γ than that at $J = 28\hbar$, which is attributed to the value of deformation in a hot compound nucleus generally increasing with its angular momentum. The hot compound nucleus ^{32}S is generated from the fusion reaction $^{20}\text{Ne} + ^{12}\text{C}$ at 145 MeV with $J = 20\hbar$. Comparing with the GDR spectrum with the inclusive

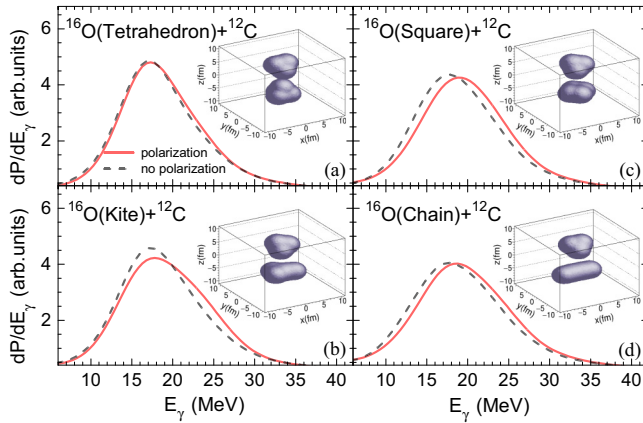


FIG. 5. The GDR spectra obtained within the EQMD model for ^{28}Si nucleus from central $^{16}\text{O} + ^{12}\text{C}$ collisions at 125 MeV. Solid lines denote the calculations with polarization for the initial projectile nuclei ^{16}O , and dotted lines correspond to those without polarization. The density distributions for ^{16}O and ^{12}C at $t = 0$ fm/c are shown in the inset plots.

configurations in the projectile ^{20}Ne , the lower energy peak component with the Woods-Saxon configuration is clearly seen, which suggests that the hot compound nucleus has a larger deformation. This also confirms that the GDR spectra in the hot compound nuclei are sensitive to the geometric configuration of the projectile.

D. Polarization effects

In this section, we will further investigate the effects of α -clustering configurations on the GDRs in hot compound systems from the fusion reactions induced by α -clustering nuclei with polarization.

As an example, the GDR spectra in the hot compound nucleus ^{28}Si from the fusion reactions of $^{16}\text{O} + ^{12}\text{C}$ at incident energy 125 MeV are plotted in Fig. 5. For the initial α -conjugate projectile ^{16}O , there are four different geometric structures including tetrahedron, kite, square, and chain configurations. The solid lines correspond to the calculations with polarization for the initial projectile ^{16}O , and the dotted lines show the result without polarization. The density distributions of the system at the initial states, i.e., $t = 0$ fm/c, where the projectiles ^{16}O with different α -clustering configurations are polarized so that their longest axes are located along the x axis direction, are shown as inset plots. The different α -clustering configurations can be clearly observed from these inset figures in Figs. 5(a)–5(d). The polarized collisions with special incident direction will amplify the asymmetry of phase space from incident channel configurations, while the nucleons' distribution will be more symmetric for nonpolarized collisions.

A comparison with the GDR spectrum without polarization in the projectile ^{16}O shows that the GDR peak position with polarization moves to the right, i.e., it is located at a higher E_γ , especially for the kite, square, and chain configurations in the projectile ^{16}O . The reason is that these α -clustering geometric structures are much more asymmetric in the phase space than the tetrahedron configurations. Therefore, the GDR spectrum in hot compound nuclei is not only sensitive to the α -clustering configurations of the projectile, but also closely related to the distribution of geometric structure in phase space.

IV. SUMMARY

In summary, the present work focuses on the effects of α -clustering configurations on the giant dipole resonance in hot compound nuclei. Under the framework of an extended quantum molecular dynamics model, the GDR spectra in ^{28}Si , ^{47}V , and ^{32}S , populated from the fusion reactions $^{16}\text{O} + ^{12}\text{C}$, $^{20}\text{Ne} + ^{27}\text{Al}$, as well as $^{20}\text{Ne} + ^{12}\text{C}$ respectively, were calculated. The results show that the computed GDR spectra in the hot nucleus ^{28}Si are composed of two peaks, which are very consistent with the experimental measurement and are remarkably sensitive to the configurations of projectile ^{16}O , including the linear chain, kite, square, and tetrahedron configurations. Additionally, the configuration sensitivity of the GDRs shows a tendency to gradually increase with angular momentum. But for the fusion system induced by ^{20}Ne , the GDRs in ^{47}V and ^{32}S are mostly independent of the α -clustering configurations of ^{20}Ne , which may be attributed to their much more similar geometric structures between the square pyramid and trigonal bipyramid configurations at the initial states. The GDRs in hot compound nuclei induced by the projectiles with Woods-Saxon distribution and polarization were also studied. Interestingly, we found that the GDR lineshapes in hot compound systems are sensitive to the geometric distributions of the projectile in phase space. Therefore, the present work clarifies that the GDR can be taken as an experimental observable to extract information on the configurations of reaction systems.

ACKNOWLEDGMENTS

This work is supported by the National Natural Science Foundation of China under Contracts No. 12105053, No. 11890710, No. 11890714, No. 12147101, No. 11875066, No. 11925502, No. 11961141003, and No. 11935001, by the Strategic Priority Research Program of CAS under Grant No. XDB34000000, by the National Key R&D Program of China under Grants No. 2016YFE0100900 and No. 2018YFE0104600, and by the Guangdong Major Project of Basic and Applied Basic Research No. 2020B0301030008.

- [1] M. Freer and A. C. Merchant, *J. Phys. G* **23**, 261 (1997).
 [2] X. G. Cao and Y. G. Ma, *Chin. Sci. Bull.* **60**, 1557 (2015).
 [3] S. A. Sofianos, R. M. Adam, and V. B. Belyaev, *Phys. Rev. C* **84**, 064304 (2011).

- [4] W. von Oertzen, M. Freer, and Y. Kanada-En'yo, *Phys. Rep.* **432**, 43 (2006).
 [5] K. Ikeda, N. Takigawa, and H. Horiuchi, *Prog. Theor. Phys. Suppl.* **E68**, 464 (1968).

- [6] W. B. He, Y. G. Ma, X. G. Cao, X. Z. Cai, and G. Q. Zhang, *Phys. Rev. Lett.* **113**, 032506 (2014).
- [7] W. B. He, Y. G. Ma, X. G. Cao, X. Z. Cai, and G. Q. Zhang, *Phys. Rev. C* **94**, 014301 (2016).
- [8] B. S. Huang and Y. G. Ma, *Phys. Rev. C* **103**, 054318 (2021).
- [9] L. Liu and P. W. Zhao, *Chin. Phys. C* **36**, 818 (2012).
- [10] A. S. Umar, J. A. Maruhn, N. Itagaki, and V. E. Oberacker, *Phys. Rev. Lett.* **104**, 212503 (2010).
- [11] J.-P. Ebran, E. Khan, T. Nikšić, and D. Vretenar, *Nature (London)* **487**, 341 (2012).
- [12] M. Huang, A. Bonasera, S. Zhang *et al.*, *Chin. Phys. C* **45**, 024003 (2021).
- [13] D. J. Marín-Lámbarri, R. Bijker, M. Freer, M. Gai, Tz. Kokalova, D. J. Parker, and C. Wheldon, *Phys. Rev. Lett.* **113**, 012502 (2014).
- [14] M. Chernykh, H. Feldmeier, T. Neff, P. von Neumann-Cosel, and A. Richter, *Phys. Rev. Lett.* **98**, 032501 (2007).
- [15] Y. Kanada-En'yo, M. Kimura, and A. Ono, *Prog. Theor. Exp. Phys.* **2012**, 01A202 (2012).
- [16] P. Adsley, M. Heine, D. G. Jenkins *et al.*, *Phys. Rev. Lett.* **129**, 102701 (2022).
- [17] S. Elhatisari, E. Epelbaum, H. Krebs, T. A. Lähde, D. Lee, N. Li, B. N. Lu, Ulf-G. Meißner, and G. Rupak, *Phys. Rev. Lett.* **119**, 222505 (2017).
- [18] R. Smith, T. Kokalova, C. Wheldon, J. E. Bishop, M. Freer, N. Curtis, and D. J. Parker, *Phys. Rev. Lett.* **119**, 132502 (2017).
- [19] C. Romero-Redondo, S. Quaglioni, P. Navrátil, and G. Hupin, *Phys. Rev. Lett.* **117**, 222501 (2016).
- [20] Y. Liu and Y. L. Ye, *Nucl. Sci. Tech.* **29**, 184 (2018).
- [21] Y. G. Ma and S. Zhang, Influence of Nuclear Structure in Relativistic Heavy-Ion Collisions, in *Handbook of Nuclear Physics*, edited by I. Tanihata, H. Toki, and T. Kajino (Springer, Singapore, 2022).
- [22] S. Zhang, Y. G. Ma, J. H. Chen, W. B. He, and C. Zhong, *Phys. Rev. C* **95**, 064904 (2017).
- [23] Y. Z. Wang, S. Zhang, and Y. G. Ma, *Phys. Lett. B* **831**, 137198 (2022).
- [24] Y. A. Li, D. F. Wang, S. Zhang, and Y. G. Ma, *Phys. Rev. C* **104**, 044906 (2021).
- [25] J. J. He, W. B. He, Y. G. Ma, and S. Zhang, *Phys. Rev. C* **104**, 044902 (2021).
- [26] D. F. Wang, S. Zhang, and Y. G. Ma, *Phys. Rev. C* **103**, 024901 (2021).
- [27] B. S. Huang, Y. G. Ma, and W. B. He, *Phys. Rev. C* **95**, 034606 (2017).
- [28] C. Z. Shi and Y. G. Ma, *Nucl. Sci. Tech.* **32**, 66 (2021).
- [29] L. Shen, B. S. Huang, and Y. G. Ma, *Phys. Rev. C* **105**, 014603 (2022).
- [30] Z. X. Ren, P. W. Zhao, and J. Meng, *Phys. Lett. B* **801**, 135194 (2020).
- [31] Z. X. Ren, S. Q. Zhang, P. W. Zhao, N. Itagaki, J. A. Maruhn, and J. Meng, *Sci. China Phys. Mech. Astron.* **62**, 112062 (2019).
- [32] X. Y. Li, Z. J. Wu, and L. Guo, *Sci. China Phys. Mech. Astron.* **62**, 122011 (2019).
- [33] Y. Kanada-En'yo and H. Horiuchi, *Prog. Theor. Phys.* **93**, 115 (1995).
- [34] M. Kimura, T. Suhara, and Y. Kanada-En'yo, *Eur. Phys. J. A* **52**, 373 (2016).
- [35] A. Tohsaki, H. Horiuchi, P. Schuck, and G. Röpke, *Phys. Rev. Lett.* **87**, 192501 (2001).
- [36] Y. Funaki, H. Horiuchi, and A. Tohsaki, *Prog. Part. Nucl. Phys.* **82**, 78 (2015).
- [37] B. Zhou, Y. Funaki, H. Horiuchi, Z. Ren, G. Roepke, P. Schuck, A. Tohsaki, C. Xu, and T. Yamada, *Phys. Rev. Lett.* **110**, 262501 (2013).
- [38] A. Bracco, F. Camera, M. Mattiuzzi *et al.*, *Phys. Rev. Lett.* **74**, 3748 (1995).
- [39] M. Mattiuzzi, A. Bracco, F. Camera *et al.*, *Nucl. Phys. A* **612**, 262 (1997).
- [40] D. Santonocito and Y. Blumenfeld, *Eur. Phys. J. A* **56**, 279 (2020).
- [41] J. A. Maruhn, P. G. Reinhard, P. D. Stevenson, J. R. Stone, and M. R. Strayer, *Phys. Rev. C* **71**, 064328 (2005).
- [42] D. Pandit, D. Mondal, B. Dey, S. Bhattacharya, S. Mukhopadhyay, S. Pal, A. De, and S. R. Banerjee, *Phys. Rev. C* **95**, 034301 (2017).
- [43] S. S. Wang, Y. G. Ma, X. G. Cao, W. B. He, H. Y. Kong, and C. W. Ma, *Phys. Rev. C* **95**, 054615 (2017).
- [44] N. F. Lattoofi and Ali A. Alzubadi, *Int. J. Mod. Phys. E* **29**, 2050084 (2020).
- [45] B. S. Ishkhanov and S. Yu. Troshchiev, *Moscow Univ. Phys. Bull.* **66**, 325 (2011).
- [46] F. Niu, P. H. Chen, and Z. Q. Feng, *Nucl. Sci. Tech.* **32**, 103 (2021).
- [47] K. X. Cheng, J. Pu, Y. T. Wang, Y. F. Guo, and C. W. Ma, *Nucl. Sci. Tech.* **33**, 132 (2022).
- [48] D. Pandit, S. Mukhopadhyay, S. Bhattacharya, S. Pal, A. De, S. Bhattacharya, C. Bhattacharya, K. Banerjee, S. Kundu, T. K. Rana, A. Dey, G. Mukherjee, T. Ghosh, D. Gupta, and S. R. Banerjee, *Phys. Rev. C* **81**, 061302(R) (2010).
- [49] B. Dey, S. S. Wang, D. Pandit, S. Bhattacharya, X. G. Cao, W. B. He, Y. G. Ma, N. Q. Hung, and N. D. Dang, *Phys. Rev. C* **102**, 031301(R) (2020).
- [50] D. R. Chakrabarty, N. Dinh Dang, and V. M. Datar, *Eur. Phys. J. A* **52**, 143 (2016).
- [51] J. Aichelin, *Phys. Rep.* **202**, 233 (1991).
- [52] C. Hartnack, R. K. Puri, J. Aichelin, J. Konopka, S. A. Bass, H. Stöcker, and W. Greiner, *Eur. Phys. J. A* **1**, 151 (1998).
- [53] T. Maruyama, K. Niita, and A. Iwamoto, *Phys. Rev. C* **53**, 297 (1996).
- [54] S. S. Wang, X. G. Cao, T. L. Zhang, H. W. Wang, G. Q. Zhang, D. Q. Fang, C. Zhong, C. W. Ma, W. B. He, and Y. G. Ma, *Nucl. Phys. Rev.* **32**, 24 (2015).
- [55] Y. T. Cao, X. G. Deng, and Y. G. Ma, *Phys. Rev. C* **106**, 014611 (2022).
- [56] K. Wang, Y. G. Ma, G. Q. Zhang, X. G. Cao, W. B. He, and W. Q. Shen, *Phys. Rev. C* **95**, 014608 (2017).
- [57] C. Q. Guo, Y. G. Ma, W. B. He, X. G. Cao, D. Q. Fang, X. G. Deng, and C. L. Zhou, *Phys. Rev. C* **95**, 054622 (2017).
- [58] M. Goldhaber and E. Teller, *Phys. Rev.* **74**, 1046 (1948).
- [59] W. D. Myers, W. J. Svatccki, T. Kodama, L. J. El-Jaick, and E. R. Hilf, *Phys. Rev. C* **15**, 2032 (1977).
- [60] V. Baran, M. Cabibbo, M. Colonna, M. Di Toro, and N. Tsoneva, *Nucl. Phys. A* **679**, 373 (2001).

- [61] B. Zhou, Y. Funaki, H. Horiuchi, Y.-G. Ma, G. Röpke, P. Schuck, A. Tohsaki, and T. Yamada (private communication).
- [62] B. Dey, C. Ghosh, D. Pandit, A. K. Rhine Kumar, S. Pal, V. Nanal, R. G. Pillay, P. Arumugam, S. De, G. Gupta, H. Krishnamoorthy, E. T. Mirgule, S. Pal, and P. C. Rout, *Phys. Rev. C* **97**, 014317 (2018).
- [63] D. Kusnezov, Y. Alhassid, and K. A. Snover, *Phys. Rev. Lett.* **81**, 542 (1998).
- [64] I. Mukul, A. Roy, P. Sugathan, J. Gehlot, G. Mohanto, N. Madhavan, S. Nath, R. Dubey, I. Mazumdar, D. A. Gothe, M. Kaur, A. K. Rhine Kumar, and P. Arumugam, *Phys. Rev. C* **88**, 024312 (2013).